Optical resonances in bimetallic clusters and their relation to the electronic structure

C. Yannouleas, P. Jena, and S. N. Khanna
Department of Physics, Virginia Commonwealth University, P.O. Box 2000, Richmond, Virginia 23284
(Received 12 February 1992)

The optical response of bimetallic clusters of composition YA_x, where A is an alkali metal and Y is a monovalent or divalent impurity, is studied by using the random-phase approximation upon a two-step jellium ionic background. With respect to the homologous pure clusters, the optical properties of mixed clusters are found to exhibit conspicuous variations that are directly related to corresponding drastic modifications in the electronic structure induced by the impurity atom. Parallel *ab initio* calculations are performed to test the adequacy of the two-step jellium model.

I. INTRODUCTION

One of the most interesting aspects of metal clusters is that their ground-state properties (e.g., the stability, ionization potentials, electron affinities) exhibit discontinuities as a function of size that are strikingly similar to those observed in corresponding quantities (e.g., in the separation energies for protons and neutrons) in nuclear physics. The observation by Knight and his co-workers[1,2] that the abundances in the mass spectra of alkali-metal clusters exhibited pronounced peaks or steps at 2,8,20,40,58,92,138,... atoms, in close resemblance with the magic numbers in nuclear physics, constituted a major development in our understanding of cluster physics. Indeed, it lent support to the jellium-background model and to a view of metal-cluster properties as due primarily to fully delocalized valence electrons that are, however, confined inside the finite volume of the cluster. Thus, the enhanced stability of the magic alkali-metal clusters was explained as an effect of electronic shell structure, just as the enhanced stability of magic nuclei is due to the nuclear shell structure.[3]

The observation of these discontinuities offered the first indication that clusters constitute a link between nuclear physics and condensed matter physics (for a review, cf. Refs. 4 – 6). Indeed, metal clusters provide an avenue where concepts from nuclear structure and nuclear dynamics can be applied in the electron-volt energy range. In particular, the shell structure in clusters can be studied by considering the effective central potential field that binds the delocalized valence electrons. In analogy with nuclear physics, a Woods-Saxon external potential was first considered,[1] but it soon became apparent that more appropriate central potentials can be constructed self-consistently starting from the jellium-background approximation.[7,8] In this approach, the ionic lattice is replaced by a uniform, positive, spherical density, while the Coulomb interaction between the delocalized electrons is treated in the local-density approximation (LDA). Then the effective field is specified self-consistently by minimizing the total energy of the valence electrons according to the Kohn-Sham method.[9]

To illustrate how the discontinuities in the ground-state properties relate to the shell structure induced by the effective potential, we have calculated the ionization potentials of pure potassium clusters in the spherical jellium approximation. They are displayed in Fig. 1 along with the corresponding energies of the highest occupied molecular orbitals (HOMO). The largest ionization potentials at 8, 18, and 20 electrons are accompanied by sharp drops, while the HOMO levels exhibit the opposite behavior in keeping with Koopman's theorem. This behavior reflects the filling up of the $1p$, $1d$, and $2s$ electronic shells, respectively. Figure 2 displays the electron affinities for small potassium clusters. Since the added electron goes into the lowest unoccupied molecular orbital (LUMO), the LUMO levels also reflect sharp

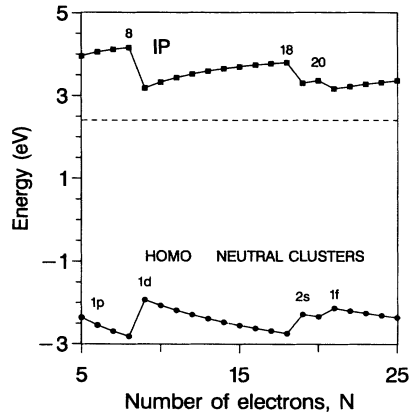

FIG. 1. The ionization potentials (IP's) for the pure series K_x calculated in the spherical jellium approximation. The corresponding energies of the $1p$, $1d$, $2s$, and $1f$ highest occupied molecular orbitals (HOMO) are also shown. The maximum IP's appear when an electronic shell is closed at $N = 8$, 18, and 20 electrons ($N = x$). All the IP's have values higher than the bulk work function of potassium at 2.4 eV (dashed line).

 ©1992 The American Physical Society

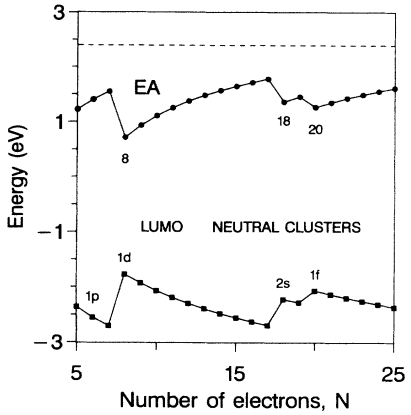

FIG. 2. The electron affinities (EA's) for the pure series K_x calculated in the spherical jellium approximation. The corresponding energies of the $1p$, $1d$, $2s$, and $1f$ lowest *un*occupied molecular orbitals (LUMO) are also shown. The minimum EA's appear when an electronic shell is closed at $N = 8$, 18, and 20 electrons ($N = x$). All the EA's have values lower than the bulk work function of potassium at 2.4 eV (dashed line).

changes in the electron affinity at the electronic magic numbers 8,18,20,.... Thus the ionization potential (electron affinity) and the HOMO (LUMO) levels carry the physics in jellium clusters.

The similarities between metal-cluster and nuclear physics extend beyond the ground-state properties. Indeed, the optical response of metal microclusters exhibits substantial analogies with corresponding photonuclear processes.[6] In particular, the photoabsorption in metal clusters proceeds via the excitation of a dipole plasma mode where the valence electrons move collectively against the jellium positive background. This process is quite analogous to the well-known giant dipole resonance in nuclei, where the protons move against the neutrons.[10]

Detailed studies of the photoabsorption profiles in alkali-metal clusters have been carried out using the time-dependent extension of the local-density approximation (TDLDA),[11–13] or using techniques closely related to the nuclear many-body problem.[14–16] In particular, the matrix-RPA (random-phase approximation) was adapted[14,15] to the case of spherical, closed-shell clusters. For specific mass numbers and species, like neutral Na_{20} and Na_{40}, this method predicted multipeak photoabsorption profiles, more complex than the simple one-peak profile expected from the Mie theory[17] for the charge oscillations of a classical metal sphere (ellipsoidal model[18,19]). Such profiles have been recently observed experimentally.[18,20] They represent quantum size effects due to the discreteness of the single-particle levels and their bunching into electronic shells.

Unlike the ground-state properties, which reflect directly the level bunching into shells, the optical response depends upon energy differences between unoccupied and occupied electronic orbitals, and thus it reflects the shell structure in a less obvious way. However, this paper will show that a well-defined relationship between trends in ground-state properties and trends in excited-state properties can be established as the shell structure varies from the pure to the mixed metallic aggregates.

Indeed, selective changes in the position of single-particle levels can be reflected both in the electronic and in the optical properties of clusters. To this end, a means is needed for altering the electronic structure away from the square-well prototype, familiar from the case of pure alkali-metal clusters. In the case of metallic clusters, an efficient way for inducing modifications in the electronic structure is the alteration of their chemical composition. In particular, with respect to the pure clusters, the impurity in bimetallic clusters, like MgK_x and NaK_x, induces unequal shifts in the single-particle levels.[21–25] Specifically, the s levels are substantially influenced, while the rest of the angular momenta remain relatively unaffected. The associated shifts are drastic and can be reflected in a conspicuous way in concerted variations of both the ground-state properties and the optical properties. The aim of the present paper is to study these modifications and their interconnection. To this end, both molecular methods and nuclear methods, adapted to the case of compound aggregates, will be utilized.

We describe the theoretical formulation in Sec. II. In Sec. III we compare the molecular and jellium approaches. The results are presented in Sec. IV, and the conclusions are drawn in Sec. V.

II. THEORETICAL TOOLS AND METHODOLOGY

A. Two-step jellium background

Before proceeding to study the properties of mixed clusters, we need to develop an adequate description of the associated static, effective potentials. Apart from the calculation of ground-state properties, the effective potentials are needed as an input into the matrix-RPA within the local-density approximation utilized here. Specifically, the influence of the average field upon the RPA equations is manifested through the energy differences from the unoccupied to the occupied single-particle orbitals (particle-hole transitions). For mixed clusters, such effective potentials can be determined within the framework of a modified jellium background.

For homonuclear clusters, the effective potential is determined by replacing the ionic charges by a homogeneous positive background of density n_0 which, in the absence of any other information, is assumed to have the bulk value Z/Ω_0 (Z being the atomic valence and Ω_0 the atomic volume). The radius R of the positive background is determined by the number N_a of atoms in the cluster,

$$\frac{4\pi}{3}R^3\, n_0 = N_a\, Z = N. \tag{1}$$

N is naturally the total number of delocalized electrons in the cluster.

Since metal clusters occupy a finite volume, the rela-

tive spacing of the electron energy levels will of course depend upon the value of n_0. Empirical evidence suggests that, for pure sodium and potassium clusters, the bulk values of n_0 are good enough. However, there is no apparent reason why the cluster ion density n_0 should be the same as the bulk density. A more refined procedure would choose the value of n_0 in small clusters in such a way that the level spacings calculated in the jellium model correspond as closely as possible to those obtained from self-consistent-field–linear combination of atomic orbitals–molecular orbitals (SCF-LCAO-MO) calculations on optimized cluster geometries. Then, comparisons can be made with clusters of different sizes to see how the average background density n_0 evolves and approaches the bulk value.

For a compound cluster containing the heteroatom (impurity I) at the center of the otherwise homonuclear host (H) cluster, the positive background n_+ will be modified as follows:

$$n_+ = n_0^I\,\theta(R_I - r) + n_0^H\,\theta(r - R_I)\theta(R_H - r)\ , \quad (2)$$

where $\theta(R - r) = 0$ for $r > R$ and 1 for $r < R$ (see Fig. 3).

The use of the two-step jellium model (2) is particularly useful in describing large heteroclusters, since *ab initio* methods of the type described earlier are restricted to small clusters due to limitations of the present computational resources.

In the case of the two-step distribution (2), an initial choice for the electronic densities could be the corresponding bulk values. However, although this choice preserves the overall trend in the abundance spectra, it leads to significant discrepancies with the experimental observations in the case of divalent impurities.[22] Best known is the case of the series MgK_x, where this procedure predicts strong abundance maxima for both MgK_6 and MgK_8,[23] even though only MgK_8 exhibits a maximum in the experimental abundances.[26]

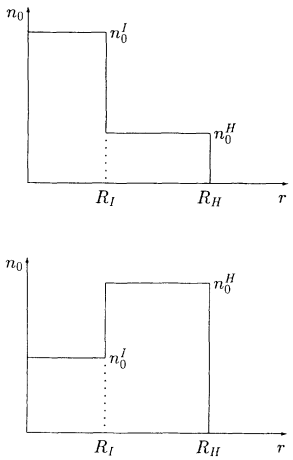

FIG. 3. Schematic representation of the two-step positive jellium background, with the impurity (I) occupying the central region. Both cases of an impurity with a larger ($n_0^I > n_0^H$) and a smaller ($n_0^I < n_0^H$) electronic density than the host are shown.

In the present work, we will adopt a more flexible approach, and, we will assign to the density n_0^I of the divalent impurity a set of varying values, while retaining the bulk value for the alkali-metal atoms. A comparison with the observation for both the ground-state and optical properties will determine the best values for the model. In parallel, comparison with molecular-orbital calculations can yield information about the adequacy of the assumed geometrical arrangement for the ionic cores.

B. Random-phase approximation

The description of the collective excitations of bimetallic clusters, which we will present below, follows closely the method used to describe plasma resonances in pure alkali-metal clusters.[14,15] A discrete particle-hole basis is constructed out of the single-particle energies for the Hamiltonian,

$$H_0 = T + U(r)\ , \quad (3)$$

where $U(r)$ is the static effective potential resulting from the two-step jellium background and T is the kinetic energy of the valence electrons. Then the total Hamiltonian $H = H_0 + V$, sum of H_0 and of the residual particle-hole interaction V specified in the local-density approximation (LDA), is diagonalized using the matrix-RPA (for details, cf. Ref. 15).

The RPA eigenstates $|n\rangle$ are formed as a linear superposition of particle-hole excitations in terms of the forward-going and backward-going amplitudes. Since the RPA preserves the Thomas-Reiche-Kuhn (energy-weighted) sum rule $S(E1) = N\hbar^2e^2/2m$, the dipole transition probabilities $B(E1, 0 \rightarrow n)$ and associated eigenvalues E_n obey the relation

$$\sum_n f_n = 1\ , \quad (4)$$

where the oscillator strengths f_n per delocalized electron are defined as

$$f_n = \frac{E_n\,B(E1, 0 \rightarrow n)}{S(E1)}. \quad (5)$$

This result is also valid for the unperturbed particle-hole excitations.

C. Molecular calculations

The electronic structure calculations were carried out within the linear combination of atomic orbitals–molecular orbitals (LCAO-MO) approach.[27] The molecular wave function Ψ is expressed as a linear combination of atomic orbitals ϕ_k centered at the atomic sites k. The orbitals ϕ_k are themselves expanded as a sum of the Gaussian functions g_j,

$$\Psi = \sum_k a_k\phi_k = \sum_k a_k \sum_j c_j^k g_j^k = \sum_{kj} d_{kj} g_j^k\ . \quad (6)$$

The coefficient d_{kj} are determined via a solution of the

Rayleigh-Ritz equation

$$(H - E)\Psi = 0 \,, \tag{7}$$

where H is the many-body Hamiltonian consisting of the kinetic energy T, the ionic attraction term $V_{\rm ion}$, the electron hartree repulsion V_H, and the electron exchange-correlation term $V_{\rm xc}$, namely,

$$H = T + V_{\rm ion} + V_H + V_{\rm xc} \,. \tag{8}$$

In all our studies, the exchange-correlation contributions have been included within the density-functional approach.[28] Equation (7) then reduces to the Kohn-Sham equations,[9]

$$(-\tfrac{1}{2}\nabla^2 + V_{\rm ion} + V_H + V_{\rm xc}^{\sigma})\,\Psi_{\sigma}^{\nu} = \epsilon_{\sigma}^{\nu}\,\Psi_{\sigma}^{\nu} \,, \tag{9}$$

where σ is the spin index (up or down) and ν is the eigenvalue index.

We have used the form of the exchange-correlation potential proposed by Ceperley and Alder.[29] Further, the inner cores have been replaced by norm-conserving nonlocal pseudopotentials. The particular form of pseudopotentials we have used are the ones proposed by Bachelet, Hamann, and Schlüter.[30] These are based on accurate local-density calculations on atoms, have optimum transferability, and their parametrized form is easily adaptable for molecular applications.

To carry out electronic structure calculations, one needs the Gaussian basis functions g_j. Since we are using pseudopotentials, the available Gaussian basis functions for Hartree-Fock and other all electron studies are not appropriate. We therefore developed our own basis sets by solving the atomic equation on a numerical mesh. The numerical atomic functions were fitted nonlinearly to a combination of Gaussian functions. For Na, K, Mg, and Zn, the basis sets consisted of $(3s, 2p)$, $(4s, 3p)$, $(4s, 2p)$, and $(4s, 2p, 5d)$ basis functions, respectively. All the basis sets were not contracted. The basis sets were tested by comparing the one-electron levels and the total energy based on the basis sets with the corresponding quantities obtained via numerical integration of the Schrödinger equation. The basis sets were also tested for their overcompleteness by carrying out atomic calculations with an extra set of basis functions at varying distances. The changes in total energy were minimal.

Using the above Gaussian functions, Eq. (9) was solved self-consistently. The total energy was calculated via the expression[31]

$$\begin{aligned} E = &\sum_{\sigma,\nu} \langle \Psi_{\sigma}^{\nu} | (-\tfrac{1}{2}\nabla^2 + V_{\rm ion}) | \Psi_{\sigma}^{\nu} \rangle \\ &+ \tfrac{1}{2} \int\int \frac{\rho(\mathbf{r})\rho(\mathbf{r}')}{|\mathbf{r} - \mathbf{r}'|} d\mathbf{r}\, d\mathbf{r}' + \int \epsilon_{\rm xc}(\mathbf{r})\rho(\mathbf{r}) d\mathbf{r} \\ &+ \sum_{1 \le i < j \le N} \frac{Z_i Z_j}{|\mathbf{R}_i - \mathbf{R}_j|} \,, \end{aligned} \tag{10}$$

where $\rho_{\sigma}(\mathbf{r}) = \sum_{\nu} |\Psi_{\sigma}^{\nu}(\mathbf{r})|^2$ and $\rho(\mathbf{r}) = \sum_{\sigma} \rho_{\sigma}(\mathbf{r})$ denotes the electron density at the point $\mathbf{r}$. $\epsilon_{\rm xc}(\mathbf{r})$ denotes the exchange-correlation energy per electron, and Z_i is the charge of the ions located at $\mathbf{R}_i$. The ground-state geometries were obtained by minimizing the total energy for given symmetry constraints.

III. COMPARISON OF MOLECULAR AND JELLIUM CALCULATIONS

To test the reliability of the two-step jellium model, we have carried out parallel molecular calculations and have compared the electronic structures resulting from the two approaches. Specifically, we present here results for the mixed aggregates MgK_8, $ZnNa_8$, and MgK_6. In the case of the molecular calculations, the geometry was assumed to be a centered cubic for MgK_8 or $ZnNa_8$ and a centered octahedron for MgK_6. For the jellium calculations, the densities n_0^I and n_0^H were assumed to be equal to the corresponding bulk values.

For these two geometries, the molecular electronic configurations are of the type $(1a_{1g})^2\ (1t_{1u})^6\ (2a_{1g})^2$ and $(1a_{1g})^2\ (1t_{1u})^6$, respectively. Comparison with the jellium calculations is based on the correspondence $1s \rightarrow 1a_{1g}$, $1p \rightarrow 1t_{1u}$ $2s \rightarrow 2a_{1g}$, and $1d \rightarrow (1d_t + 1d_e)$. Generally, the gap inside the molecular d manifold is much smaller than the gap between the major shells, and it can be overlooked for the purpose of the present comparison. To illustrate the validity of this correspondence between the orbital levels, we have decomposed the molecular wave functions in angular-momentum orbitals with respect to the ionic charge center. For the case of $ZnNa_8$, the coefficient of the spherical harmonic with the maximum contribution C_L is listed in Table I. Even for the least favorable case of the d orbitals, the corresponding coefficient C_L is very large, namely, 0.980.

Table I also lists the energy spectra. It is apparent that the agreement between molecular and two-step jellium calculations is very good. In particular, both calculations reproduce the downward shift of the $2s$ level below the $1d$ level, and thus are able to account for the principal experimental finding, namely the appearance of the new magic number $N = 10$ electrons.[32]

This agreement between electronic configurations persists also in the case of MgK_6 and MgK_8, as Table II and Fig. 4 illustrate, respectively. Such an agreement between molecular and jellium methods lends support to the usefulness of the two-step jellium background as an alternative approach in describing metal heteroclusters, a fact particularly relevant in the case of larger mass numbers ($>$ 10) where computer limitations restrict the applicability of *ab initio* methods.

TABLE I. Molecular vs jellium levels for $ZnNa_8$. The coefficient C_L of the spherical harmonic with the largest contribution in the associated molecular orbital is also given.

Molecular			Jellium	
	eV	C_L		eV
$1a_{1g}$	−7.41	0.995 ($L = 0$)	$1s$	−6.05
$1t_{1u}$	−3.89	0.985 ($L = 1$)	$1p$	−3.68
$2a_{1g}$	−2.81	0.985 ($L = 0$)	$2s$	−2.71
$1d_t$	−1.88	0.980 ($L = 2$)	$1d$	−2.02

TABLE II. Molecular vs jellium levels for MgK_6.

Molecular	eV	Jellium	eV
$1a_{1g}$	−4.65	$1s$	−4.85
$1t_{1u}$	−2.44	$1p$	−2.86
$2a_{1g}$	−1.87	$2s$	−2.09
$1d_t$	−1.30	$1d$	−1.50

In spite of the explanation of the $N = 10$ magic number, both the calculations presented in this section fail to account for additional important features of the observed mass spectra. In particular, they fail to account for the sole observation of an abundance peak at $N = 10$ and the simultaneous absence of a peak at $N = 8$. This is because both calculations exhibit comparable gaps between the $1p$ and $2s$ levels and between the $2s$ and $1d$ levels, and thus predict an abundance peak for MgK_6 and $ZnNa_6$ as important as the peak for MgK_8 and $ZnNa_8$. This is in clear disagreement with the experimental observations for $ZnNa_x$ and MgK_x (a summary of the available experimental abundance maxima for mixed aggregates is compiled in Table III).

What this discrepancy indicates is that the actual $2s$ level is probably situated even lower than the present calculations suggest, probably close or below the $1p$ level. Since the second differences, $\Delta_2 = E(YA_{x+1}) + E(YA_{x-1}) - 2E(YA_x)$, reflect the energy gaps of the electronic spectrum, this conclusion is independent of the method considered, jellium or molecular. In the framework of the molecular orbital calculations, a better agreement between theory and experiment could be reached by considering different geometric configurations. In the framework of the two-step jellium background, it will suffice to consider the electronic density of the divalent impurity as a variable and adjust it to produce the additional necessary downward shift for the $2s$ level. This approach will be followed in Sec. IV, where a detailed comparison between the jellium results and the available experimental data for both abundances and photoabsorption spectra will be presented.

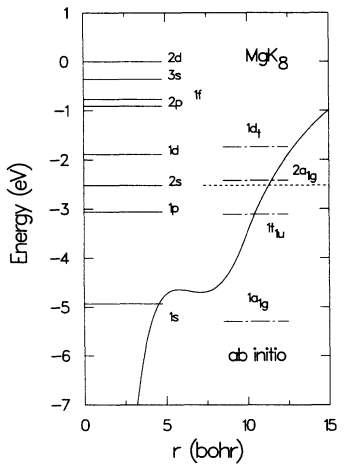

FIG. 4. Comparison of *ab initio* molecular levels (right) with two-step spherical jellium levels (left) for MgK_8. The corresponding electronic densities were taken to agree with the bulk values. The agreement between molecular and jellium calculation is very good. Unlike the case of pure K_8 or K_{10}, the $2s$ level has been shifted below the $1d$ level and has become the HOMO (dashed line). The jellium effective potential is also shown. Notice the depression that develops at the origin as a result of the Mg impurity.

TABLE III. Observed abundance maxima for heteroatom/alkali (YA_x) compound clusters.

Metals Y/A	Maxima for N = electrons
Li/Na[a]	8, 20, 40
Li/K[a]	8, 20
Mg/Na[a]	8, 10, 20
Ca/Na[a]	8, 20
Sr/Na[a]	8, 18, 20, 40
Ba/Na[a]	8, 18
Zn/Na[a]	10, 20
Eu/Na[a]	8, 18
Yb/Na[a]	8, 20, 40
Mg/K[a]	10, 20
Zn/K[a]	10, 20
Hg/K[a]	10, 21
Na/K[b]	8, 20, 40
Cs/K[b]	8, 18

[a]From Ref. 26.
[b]From Refs. 2 and 33.

This methodology is supported by the jellium calculations of Refs. 22 and 23 which found that, although the global trends presented in the abundance maxima in Table III (e.g., the disappearance of the magic N=8 and the appearance of the magic N=10) depended upon the difference of the electronic densities between impurity and host, and could be understood using bulk r_s values, the detailed behavior of a given aggregate with a divalent impurity was systematically misplaced in their calculated evolutionary sequence.

IV. RESULTS AND DISCUSSION

A. Monovalent impurity: The series NaK_x and RbK_x

We will first consider the case of a monovalent alkaline impurity, and in particular the sequence NaK_x. We compare the properties of NaK_x with those of pure K_x. Experimentally, there exist some measurements of the abundances of NaK_x as compared to the abundances of K_x.[2,33] We begin with a review of the available experimental data before describing the corresponding theoretical calculations.

1. *Single-particle levels*

As reported in Refs. 2 and 33, the presence of the Na impurity produces relative differences in the mass spectra of the doped NaK_x as compared to the series of the pure K_x. These differences are not as extreme as in the case of the series MgK_x or $ZnNa_x$, where the divalent dopant produces a new magic number for $N = 10$ electrons. Indeed, eight electrons is a well-defined magic number for both NaK_x and K_x. The relative differences appear in the area of 18–20 electrons. In particular, the rise in intensity to NaK_{19} (20 electrons) is strongly peaked in contrast to the pure K_x clusters. Moreover, in the case of Cs-doped clusters (impurity of smaller electronic density), an increase in intensity is observed up to CsK_{17} (18 electrons), followed by a drop at CsK_{18}.

These observations can be interpreted on the basis of the shell model as due to a competition of the $1d$ (18 electrons) and $2s$ (20 electrons) shell closures. Our calculations using the two-step jellium background, with the dopant occupying the central region, supports this interpretation. Figure 5 displays the second differences Δ_2 for the series of pure K_x versus the compound series NaK_x and RbK_x. We have used the values of the bulk for r_s^I, namely 4.00 a.u. for sodium (for potassium this value is 4.86 a.u., for rubidium it is 5.20 a.u.). Going from K_x to NaK_x, the peak for $N = 18$ electrons disappears, while the $N = 8$ peak remains unaffected, and no $N = 10$ peak does appear. For the series RbK_x, the $N = 18$ peak is enhanced. These trends are in good agreement with the experimentally observed abundances[2,33] described earlier (like cesium, rubidium has a lower electronic density than potassium).

Figure 5 also displays the correponding positions of the $1s, 1p, 1d, 2s$, and $1f$ levels both for $N = 8$ and for $N = 20$ electrons ($N = x + 1$, in the case of NaK_x and RbK_x). The corresponding potentials are displayed in Fig. 6.

A conspicuous effect of the heteroatom at the center[34] is the dramatic change it can cause in the effective central potential that binds the delocalized electrons compared to the case of pure clusters. Specifically, for $n_0^I > n_0^H$ (as is the case with NaK_x), a depression centered at the origin develops in the potential. This depression results in unequal shifts in the single-particle levels. The bound single-particle levels that are most influenced are the s orbitals, while the p and d orbitals remain comparatively unchanged. This is a consequence of the $\hbar^2 l(l+1)/2mr^2$ repulsive centrifugal potential that insulates the higher angular momenta from the narrow depression. The extent of the shift sustained by the s levels depends on both the difference in the electronic densities and on the size of the aggregate. This is seen from Fig. 5, where the large shifts of the s levels are clearly exhibited. In the vicinity of $N = 8$ electrons the shift of the $2s$ state is not strong enough, and the $2s$ level remains above the $1d$ level. As a result, no $N = 10$ electrons magic number appears. On

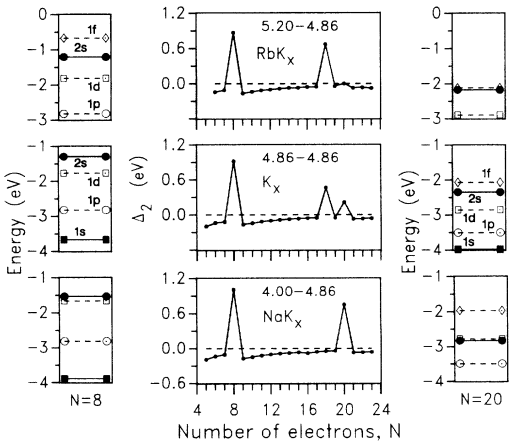

FIG. 5. Jellium second differences for the compound series RbK_x and NaK_x ($N = x + 1$) compared to the pure series K_x ($N = x$). Bulk Wigner-Seitz radii (as indicated) were used both for the host potassium and for the monovalent impurities. The peak at N =18 electrons competes with the peak at $N = 20$. An impurity with a lower electronic density (higher Wigner-Seitz radius) favors the $N = 18$ peak and vice versa in accordance with the observations for the mass spectra (Refs. 2 and 33). Notice that the peak at $N = 8$ is not influenced. This behavior is explained by the relative shift, induced by the impurity, of the $2s$ level with respect to the other orbitals, as illustrated in the left and right columns. The $2s$ level is more influenced at $N = 20$ than at $N = 8$. Left column: the jellium single-particle levels at the size $N = 8$ electrons (solid squares: $1s$; solid circles: $2s$; open circles: $1p$; open squares: $1d$; open diamonds: $1f$). Right column: the jellium single-particle levels at $N = 20$ electrons.

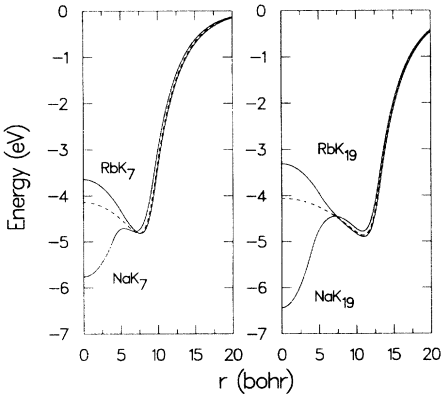

FIG. 6. The jellium effective potentials at $N = 8$ and $N = 20$ electrons for the monovalent impurities Na and Rb in a potassium host. The dashed lines correspond to the pure potassium K_8 and K_{20} cases. For an impurity with a larger electronic density (like Na), a depression develops at the origin. On the contrary, for an impurity with a smaller electronic density (like Rb), a hump develops at the origin. Due to less efficient screening, the influence of the impurity is more pronounced at $N = 20$ than at $N = 8$ in agreement with the relative shifts of the $2s$ level (cf. the corresponding single-particle spectra in Fig. 5).

the contrary, in the vicinity of $N = 20$ electrons, the $2s$ level is shifted further down and is slightly lower than the $1d$ level. As a result, the $N = 18$ electrons magic number does not appear in the sequence NaK_x.

In the case of a dopant with a smaller electronic density (the case of CsK_x or RbK_x), the opposite trends develop. Indeed, a hump (local maximum) develops now at the center of the effective potential and the $2s$ level is shifted upwards favoring the $N = 18$-electrons peak over the $N = 20$-electrons peak.

2. Ionization potentials

The movement of the $2s$ level is also reflected in the ionization potentials for the series NaK_x and RbK_x (cf. Fig. 7), as compared to the pure sequence K_x (cf. Fig. 1). Indeed, the I.P. does not show a step at NaK_{17}, in agreement with the abundances. For the case of the less dense impurity, the step at RbK_{19} is missing.

Otherwise, it is to be noticed that the value of the I.P. is almost independent of the impurity. This is because the ionization potential reflects the HOMO levels, whose energy changes very little due to the impurity. In particular, for $4 \leq x \leq 7$, the HOMO is the $1p$ level, while for $8 \leq x \leq 17$, the HOMO is the $1d$ level. This trend is in agreement with the experimental results on K_x and NaK_x presented in Ref. 35.

3. Optical response

It has been found[15] that the split-plasmon that characterizes the photoabsorption profiles of homonuclear Na_{20} and K_{20} clusters can be treated as a two-level model due to a degeneracy between the collective plasmon and a particular $2s \rightarrow 3p$ particle-hole transition. In the case of the compound NaK_{19}, the impurity at the center shifts the $2s$ level downwards, but barely affects the $3p$ level, while, at the same time, the position of the plasmon remains unchanged. As a result, the energy of the $2s \rightarrow 3p$ transition increases (cf. Fig. 8), and it is to be expected that the degree of the splitting in the photoabsorption spectrum will be affected by the presence of the Na dopant. Indeed, matrix-RPA calculations for K_{20} and NaK_{19} are displayed in Fig. 9. In the case of K_{20}, the plasmon is split into two components, while in the case of NaK_{19} there appears one dominant line with 80% of the Thomas-Reiche-Kuhn sum rule. In the case of RbK_{19}, the $2s \rightarrow 3p$ transition becomes comparatively smaller, and the extent of plasmon splitting is more pronounced, as Fig. 9 illustrates.

We have shown that the introduction of a monovalent Y impurity modifies the electronic structure of the compound YK_x with respect to the pure K_x series. In particular, in the vicinity of 20 electrons, the $2s$ level is

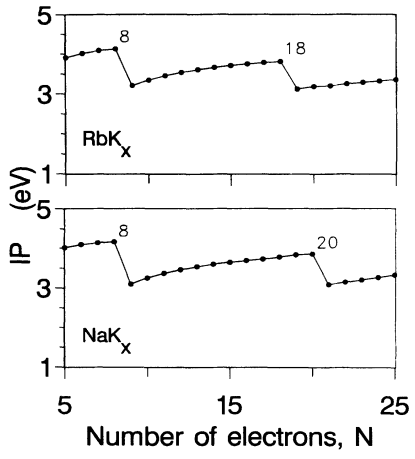

FIG. 7. The ionization potentials for the compound series RbK_x and NaK_x ($N = x + 1$). Compared to the pure K_x (cf. Fig. 1), only one step appears in the range $N = 18$–20. $N = 18$ is favored over $N = 20$ for RbK_x, while the opposite holds for NaK_x.

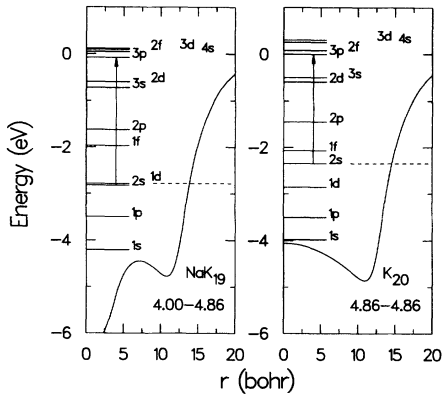

FIG. 8. The variations of the $2s \rightarrow 3p$ transition that splits the plasmon in the case of pure K_{20}, but not in the case of the mixed NaK_{19}. The associated jellium potentials are also shown. The dashed lines indicate the HOMO levels. The bulk Wigner-Seitz radii that were used are also indicated.

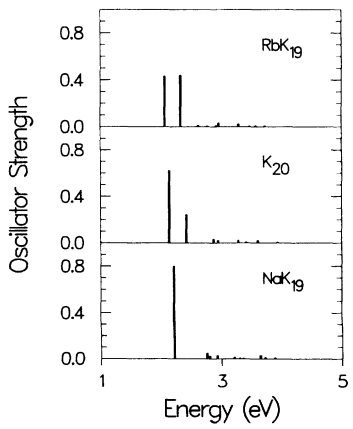

FIG. 9. RPA oscillator strengths for the compound RbK_{19}, NaK_{19}, and the pure K_{20}. Bulk Wigner-Seitz radii were used.

strongly shifted, while the $1d$ and the np levels remain relatively unaffected. This movement of the $2s$ level was shown to be reflected both in the ground-state properties as well as in the photoabsorption of the mixed aggregates.

B. Divalent impurity: The sequence $ZnNa_x$

1. Magic numbers

As discussed earlier the central depression in the potential due to the dopant shifts the $2s$ level, but leaves the $1p$ and $1d$ levels relatively unaffected. The deeper the depression, the deeper the $2s$ state is pushed down. If it is shifted below the $1d$ level, a new magic number for $N = 10$ electrons can appear for the series BA_x, where B denotes a divalent impurity ($N = x + 2$). As shown in Fig. 10 (right column), this has happened already for $r_s^I = 3.00$ in the series $B\mathrm{Na}_x$. In this case, the compound aggregate is spherical, like the case of Na_8, and in sharp contrast to the prolate Na_{10}. The competition of the peaks between $N = 8$ electrons and $N = 10$ electrons in the abundance spectra, however, is determined by the relative position of the $2s$ state with respect to both the $1d$ and $1p$ levels. Figure 10 displays the evolution of the second differences Δ_2 in the total energies of the $B\mathrm{Na}_x$ aggregates, when the Wigner-Seitz radius of the central impurity varies from 3.00 to 1.15 a.u. (for the corresponding potentials, cf. Fig. 11). A lower r_s^I favors the $N = 10$ peak. For $r_s^I = 1.15$ the $N = 8$ peak has disappeared, in agreement with the experimental data on $ZnNa_8$ (Ref. 26) (for comparison, the bulk Wigner-Seitz radius of Zn is 2.31). For $MgNa_8$, the experiment exhibits two equally sized peaks.[26] From an inspection of the trend in the second differences displayed in Fig. 10, this latter compound seems to correspond to $r_s^I = 1.90$ (for comparison, the bulk Wigner-Seitz radius of Mg is 2.65). Figure 10 also displays for $N = 10$ electrons the energy levels for the $1p$, $1d$, and $2s$ single-particle states (right column). The downward shift of the $2s$ level between the $1d$ and the $1p$ levels is well noticeable and is in agreement with the competition of the $N = 8$ and $N = 10$ peaks in the corresponding plots for the second differences.

From a comparison of the experimental mass spectra for $ZnNa_x$ and the second differences resulting from a two-step jellium model for the series $B\mathrm{Na}_x$, we infer that the best value for the Wigner-Seitz radius of the Zn impurity is 1.15 a.u. This value is substantially different from the corresponding bulk value. For the Wigner-Seitz radius of Na, we retain the bulk value of 4.00 a.u. With this choice then, we proceed to calculate the optical response of $ZnNa_8$, and compare it to the observation.[36]

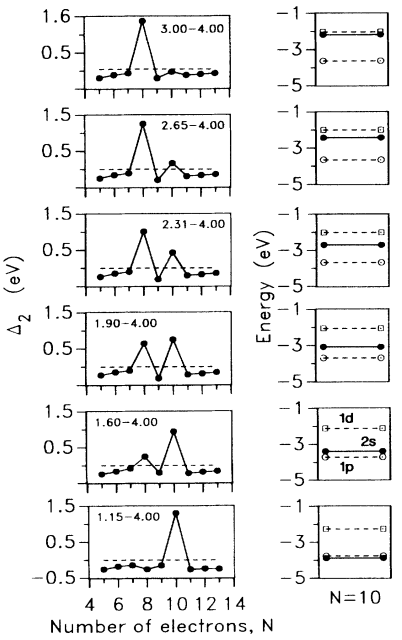

FIG. 10. Left column: jellium second differences for the series $B\mathrm{Na}_x$ ($N = x+2$), where B denotes a divalent impurity whose Wigner-Seitz radius varies from 3.00 to 1.15 a.u., as indicated in the figure. Right column: jellium single-particle spectra for $B\mathrm{Na}_8$ corresponding to the different electronic densities of the divalent impurity (solid circles: $2s$; open circles: $1p$; open squares: $1d$). The downward shift of the $2s$ orbital between the $1d$ and the $1p$ levels is apparent, and correlates with the variations in the second differences. The r_s that best reproduce the observations (cf. Table III) for the mass spectra of $ZnNa_x$ are 1.15 and 4.00.

2. Photoabsorption

$ZnNa_8$ offers another typical example of the influence of the impurity upon the photoabsorption profiles. The photoabsorption cross section of this cluster has recently been measured by Kappes *et al.*[36] A double peak has

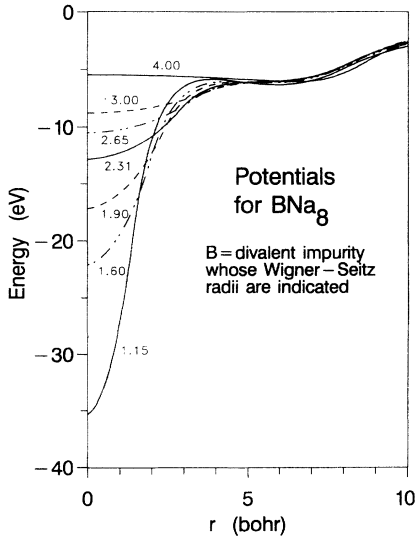

FIG. 11. Jellium potentials for $B\mathrm{Na}_8$, where B stands for a divalent impurity whose Wigner-Seitz radius varies as indicated from 4.00 to 1.15 a.u.

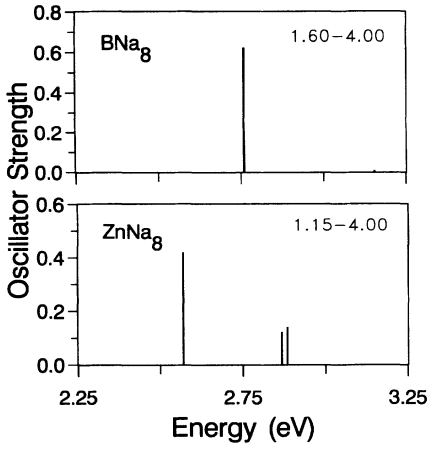

FIG. 12. RPA oscillator strengths of the mixed aggregate $B\mathrm{Na}_8$ assuming two different Wigner-Seitz radii for the divalent impurity, while retaining the associated bulk value for sodium (namely, 4.00 a.u.). The r_s that best reproduce the observed photoabsorption of ZnNa_8 (Ref. 36) are 1.15 and 4.00.

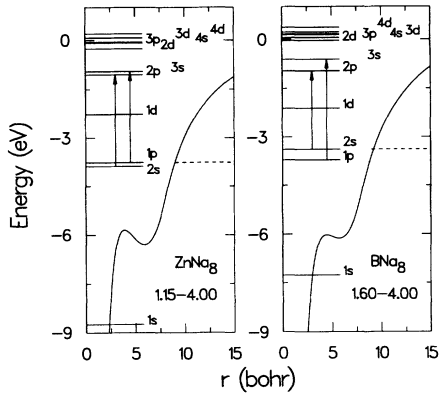

FIG. 13. The variations of the $2s \rightarrow 2p$ and $1p \rightarrow 3s$ transitions that develop as the electronic density of the divalent impurity changes. These transitions split the plasmon when the Wigner-Seitz radius of the impurity is 1.15 a.u. (cf. Fig. 12). The associated jellium potentials are also shown. The dashed lines indicate the HOMO levels. The bulk Wigner-Seitz radius of Na that was used is also indicated.

been observed: the higher component lies at 2.97 eV and carries a smaller amount of the strength than the lower component at 2.63 eV. Figure 12 displays the RPA response for the system $B\mathrm{Na}_8$ for two different values of r_s^I. For $r_s^I = 1.60$, one single line at 2.76 eV carries 62% of the TRK sum rule. In the case of $r_s^I = 1.15$, the single line is fragmented into three smaller lines. Two of these lines at higher energies (at 2.87 eV) are closely spaced and will appear as one peak after the broadening that accounts for the experimentally observed widths. Between the two of them, they carry 26% of the total strength, while the stronger line at 2.57 eV carries 42% of the strength. The variations in the photoabsorption profiles displayed in Fig. 12 depend again upon the extent of the shift sustained by the s levels. In particular, the fragmentation at the value $r_s^I = 1.15$ is due to a degeneracy that occurs between the plasmon and the $2s \rightarrow 2p$ and $1p \rightarrow 3s$ particle-hole transitions (cf. Fig. 13). A very strong shift downwards supplied by the value $r_s^I = 1.15$ is needed for this degeneracy to develop. As discussed in the earlier paragraph, the same shift accounts sufficiently well for the trend in the observed abundances of the series ZnNa_x.

V. CONCLUSION

We conclude that a two-step jellium background with the background density for the central region substantially different from the bulk value can describe sufficiently well both the optical properties and the abundances of compound clusters possessing a divalent impurity. In the case of an alkali-metal impurity, use of the bulk value seems to suffice. Specific examples have been presented on how the influence of the impurity can be accounted for within a unified framework by considering the modification of the effective average field. Approaches adapted from the nuclear many-body problem (matrix RPA) can then be immediately applied to treat the photoabsorption of compound clusters in analogy with the case of pure clusters. A strong correlation between relative differences in the electronic structure and relative differences in the optical response was found.

ACKNOWLEDGMENTS

This work was supported in part by a grant from the U.S. Army Research Office (Grant No. DAAL-03-89-K-0015). We are also grateful to F. Reuse for help with the *ab initio* calculations.

[1]W.D. Knight, K. Clemenger, W.A. de Heer, W.A. Saunders, M.Y. Chou, and M.L. Cohen, Phys. Rev. Lett. **52**, 2141 (1984).

[2]W.A. de Heer, W.D. Knight, M.Y. Chou, and M.L. Cohen, in *Solid State Physics*, edited by H. Ehrenreich, F. Seitz, and D. Turnbull (Academic, Orlando, 1987), Vol. 40, p. 93.

[3]Å. Bohr and B.R. Mottelson, *Nuclear Structure* (Benjamin, Reading, MA, 1969), Vol. I.

[4]M.L. Cohen and W.D. Knight, Phys. Today **43**(12), 42 (1990).

[5]P. Jena, C. Yannouleas, S.N. Khanna, and B.K. Rao, in *VII International Conference on Recent Progress in Many-Body Theories, Minneapolis, 1991*, edited by C.E. Campbell and E. Krotscheck (Plenum, New York, in press).

[6]R.A. Broglia, J.M. Pacheco, and C. Yannouleas, Phys. Rev. B **44**, 5901 (1991).

[7]M.Y. Chou, A. Cleland, and M.L. Cohen, Solid State Commun. **52**, 645 (1984).

[8]W. Ekardt, Phys. Rev. B **29**, 1558 (1984).
[9]W. Kohn and L.J. Sham, Phys. Rev. **140**, A1133 (1965).
[10]Å. Bohr and B.R. Mottelson, *Nuclear Structure* (Benjamin, Reading, MA, 1975), Vol. II.
[11]W. Ekardt, Phys. Rev. B **31**, 6360 (1985).
[12]M.J. Puska, R.M. Nieminen, and M. Manninen, Phys. Rev. B **31**, 3486 (1985).
[13]D.E. Beck, Phys. Rev. B **35**, 7325 (1987).
[14]C. Yannouleas, R.A. Broglia, M. Brack, and P.F. Bortignon, Phys. Rev. Lett. **63**, 255 (1989).
[15]C. Yannouleas and R.A. Broglia, Phys. Rev. A **44**, 5793 (1991).
[16]G.F. Bertsch, Comput. Phys. Commun. **60**, 247 (1990).
[17]G. Mie, Ann. Phys. (Leipzig) **25**, 377 (1908).
[18]K. Selby, V. Kresin, J. Masui, M. Vollmer, W.A. de Heer, A. Scheidemann, and W.D. Knight, Phys. Rev. B **43**, 4565 (1991).
[19]K. Selby, M. Vollmer, J. Masui, V. Kresin, W.A. de Heer, and W.D. Knight, Phys. Rev. B **40**, 5417 (1989); W.A. de Heer, K. Selby, V. Kresin, J. Masui, M. Vollmer, A. Châtelain, and W.D. Knight, Phys. Rev. Lett. **59**, 1805 (1987).
[20]S. Pollack, C.R.C. Wang, and M.M. Kappes, J. Chem. Phys. **94**, 2496 (1991); C.R.C. Wang, S. Pollack, D. Cameron, and M.M. Kappes, *ibid.* **93**, 3787 (1990).
[21]S.B. Zhang, M.L. Cohen, and M.Y. Chou, Phys. Rev. B **36**, 3455 (1987).
[22]C. Baladrón and J.A. Alonso, Physica B **154**, 73 (1988).
[23]C. Baladrón, J.A. Alonso, and M.P. Iñiguez, J. Phys. F **17**, L197 (1987).
[24]B.K. Rao and P. Jena, Phys. Rev. B **37**, 2867 (1988).
[25]P. Fantucci, V. Bonačić-Koutecký, W. Pewestorf, and J. Koutecký, J. Chem. Phys. **91**, 4229 (1989).
[26]M.M. Kappes *et al.*, in *Physics and Chemistry of Small Clusters*, Vol. 158 of *NATO Advanced Study Institute, Series B: Physics*, edited by P. Jena, B.K. Rao, and S.N. Khanna (Plenum, New York, 1987), p. 145; M.M. Kappes *et al.*, Chem. Phys. Lett. **119**, 11 (1985).
[27]W.J. Hehre, L. Radom, P.v.R. Schleyer, and J.A. Pople, *Ab initio Molecular Orbital Theory* (Wiley, New York, 1986).
[28]P. Hohenberg and W. Kohn, Phys. Rev. **136**, B864 (1964).
[29]D.M. Ceperley and B.J. Alder, Phys. Rev. Lett. **45**, 566 (1980).
[30]G.B. Bachelet, D.R. Hamann, and M. Schlüter, Phys. Rev. B **26**, 4199 (1982).
[31]F. Reuse, S.N. Khanna, V. de Coulon, and J. Buttet, Phys. Rev. B **41**, 11 743 (1990).
[32]That the presence of a divalent impurity results in the reordering of the $2s$ and $1d$ levels, so that a shell closure occurs at $N = 10$ electrons (the new magic number) instead of the usual $N = 18$, was originally described in Ref. 21. In particular, Ref. 21 calculated the single-particle spectra of the two aggregates $MgNa_6$ and $MgNa_8$ using *ab initio* molecular methods.
[33]W.A. Saunders, Ph.D. thesis, University of California, Berkeley, 1986.
[34]The impurity atom in all cases here is assumed to be in the center. In the case of several K impurities in Na, however, there is experimental and theoretical evidence that potassium tends to be on the surface [P. Ballone *et al.*, Europhys. Lett. **8**, 73 (1989)].
[35]C. Bréchignac, Ph. Cahuzac, and J.Ph. Roux, Chem. Phys. Lett. **127**, 445 (1986).
[36]M.M. Kappes *et al.* (unpublished).